Cavity–Stabilized Scramjet Analysis Using Reduced Chemical Kinetic Mechanisms

Ramin ROUZBAR, Sinan EYI

Middle East Technical University, 06800, Ankara/TURKEY

Abstract

Air-breathing propulsion is one of the important research fields of the hypersonic flow today. The objective of the present study is to develop a CFD tool to analyze the flow through Scramjets. The configuration considered is a Scramjet with single cavity recessed in the combustion chamber. Cavities are designed to enhance the mixing by means of creating a recirculation region which cause an increase in the residence time and so mixing efficiency. For this CFD tool, Euler equations and finite rate chemistry equations are used. Hydrogen-Air and Ethylene-Air combustion mechanism are considered for Scramjet combustor. For the solution of the coupled Euler and chemical reaction equations Newton-GMRES method is applied. Newton-GMRES is one of the Newton-Krylov solution methods which is a kind of Inexact Newton method.

Introduction

From mid-50's, Scramjets became main area of interest of the air-breathing propulsion systems. Since for hypersonic flow regions decelerating the flow to subsonic speeds causes significant pressure loss and temperature rise ramjets became non-profitable.[1] In Scramjets, air enters the combustion chamber at supersonic speeds and combustion occurs in supersonic flow region. One of the biggest challenges of the scramjet propulsion system is the design of the combustor since the flow must be maintained at supersonic level. Flow compressibility and reduced residence time in the combustor because of the supersonic conditions will cause poor mixing rate of the fuel-air and flame holding will be difficult. In order to overcome the low mixing efficiency cavity is used on the combustion chamber wall. The principle of the use of cavity is that by creating a circulation region in the combustor and so increasing the residence time it improves the mixing efficiency and flame holding.[2] For this study, combustion chamber of the experimental scramjet in research cell 18 at Wright-Patterson Air Force Base is taken as reference. [7]

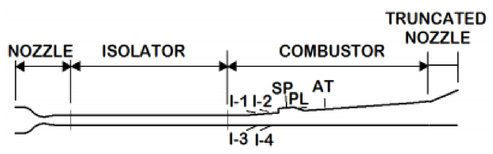

Figure 1. Schematic Scramjet

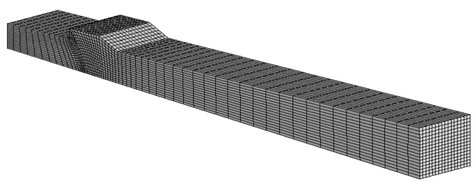

Figure 2. Combustor grid distribution

Methods

To analyze the flow in the combustion chamber, three dimensional coupled equations of Euler and finite rate chemical reactions are used.

$$\frac{\partial \hat{F}(\hat{Q})}{\partial \xi} + \frac{\partial \hat{G}(\hat{Q})}{\partial \eta} + \frac{\partial \hat{H}(\hat{Q})}{\partial \zeta} - \hat{S} = 0$$

$$\hat{Q} = \frac{1}{J}\begin{bmatrix} \rho \\ \rho u \\ \rho v \\ \rho w \\ \rho e_t \\ \rho_1 \\ \vdots \\ \rho_{K-1} \end{bmatrix}, \quad \hat{F} = \frac{1}{J}\begin{bmatrix} \rho U \\ \rho u U + \xi_x p \\ \rho v U + \xi_y p \\ \rho w U + \xi_z p \\ (\rho e_t + p) U \\ \rho_1 U \\ \vdots \\ \rho_{K-1} U \end{bmatrix}, \quad \hat{G} = \frac{1}{J}\begin{bmatrix} \rho V \\ \rho u V + \eta_x p \\ \rho v V + \eta_y p \\ \rho w V + \eta_z p \\ (\rho e_t + p) V \\ \rho_1 V \\ \vdots \\ \rho_{K-1} V \end{bmatrix}, \quad \hat{H} = \frac{1}{J}\begin{bmatrix} \rho W \\ \rho u W + \zeta_x p \\ \rho v W + \zeta_y p \\ \rho w W + \zeta_z p \\ (\rho e_t + p) W \\ \rho_1 W \\ \vdots \\ \rho_{K-1} W \end{bmatrix}, \quad \hat{S} = \frac{1}{J}\begin{bmatrix} 0 \\ 0 \\ 0 \\ 0 \\ 0 \\ \dot{\omega}_1 \\ \vdots \\ \dot{\omega}_{K-1} \end{bmatrix}$$

Spatial discretization of the flux vectors are done using upwind flux vector splitting schemes.

$$\hat{F}_{i\pm1/2,j,k} = \hat{F}^{+}{}_{i\pm1/2,j,k}\left(\hat{Q}^{-}{}_{i\pm1/2,j,k}\right) + \hat{F}^{-}{}_{i\pm1/2,j,k}\left(\hat{Q}^{+}{}_{i\pm1/2,j,k}\right)$$

$$\hat{F}^{\pm} = \pm\frac{1}{J}\,\rho c\,\frac{1}{4}(M \pm 1)^2\left(\tilde{k}_1 + \tilde{k}_2 + \tilde{k}_3\right)\begin{bmatrix} 1 \\ \frac{1}{\gamma}\left(-\tilde{U} \pm 2c\right)\tilde{k}_1 + u \\ \frac{1}{\gamma}\left(-\tilde{U} \pm 2c\right)\tilde{k}_2 + v \\ \frac{1}{\gamma}\left(-\tilde{U} \pm 2c\right)\tilde{k}_3 + w \\ \frac{\tilde{U}}{\gamma+1}\left(-\tilde{U} \pm 2c\right) + \frac{2c}{\gamma^2-1} + \frac{u^2+v^2+w^2}{2} \\ \rho_1/\rho \\ \vdots \\ \rho_{K-1}/\rho \end{bmatrix}$$

The finite rate chemistry model can be expressed as follows for K number of species and I number of the reactions:

$$\sum_{k=1}^{K} \nu'_{k,i}\chi_k \rightleftarrows \sum_{k=1}^{K} \nu''_{k,i}\chi_k \qquad (i = 1,2,..,I)$$

$$k_{fi} = A_i T^{B_i} \exp\left(-E_i/R_u T\right) \qquad k_{bi} = \frac{k_{fi}}{k_{ci}} \qquad k_{ci} = \exp\left(\left(\frac{\Delta S_i}{R} - \frac{\nabla h_i}{RT}\right)\left(\frac{P_{atm}}{RT}\right)^{\sum_{K=1}^{K}\nu_{ki}}\right)$$

$$\dot{\omega}_k = W_k \sum_{i=1}^{I}\left(\nu''_{ki} - \nu'_{ki}\right)\left(k_{fi}\prod_{k=1}^{K}[X_k]^{\nu'_{ki}} - k_{bi}\prod_{k=1}^{K}[X_k]^{\nu''_{ki}}\right)$$

In Newton-GMRES method by using the restriction given in Eq. (25) Newton's methods leads to inexact Newton method.

Table 1. Hydrogen-Air Reaction Rates

Reactions	Forward Reaction		
	A_f	B_f	E_f/R
$H_2 + M \rightleftarrows H + H + M$	2.2×10^{14}	0.0	48300
$O_2 + M \rightleftarrows O + O + M$	9.8×10^{24}	−2.5	59380
$H_2O + M \rightleftarrows OH + H + M$	3.5×10^{15}	0.0	52900
$OH + M \rightleftarrows O + H + M$	8.5×10^{18}	−1.0	50830
$H_2O + O \rightleftarrows OH + OH$	6.8×10^{13}	0.0	9240
$H_2O + H \rightleftarrows OH + H_2$	9.3×10^{13}	0.0	10250
$O_2 + H \rightleftarrows OH + O$	2.2×10^{14}	0.0	8450
$H_2 + O \rightleftarrows OH + OH$	1.8×10^{10}	1.0	4480

Table 2. Ethylene-Air Reaction Rates

Reaction	Forward Reaction		
	A_f	B_f	E_f/R
$C_2H_4 + O_2 \rightleftarrows 2CO + 2H_2$	2.10×10^{14}	0.0	18015.3
$2CO + O_2 \rightleftarrows 2CO_2$	3.48×10^{11}	2.0	10134.9
$2H_2 + O_2 \rightleftarrows 2H_2O$	3.0×10^{20}	−1.0	0.0

In order to solve the coupled Euler equations and finite rate chemistry equations Newton-GMRES is used which is an alternative method with matrix free solution technique. In Newton-GMRES method by using the restriction given, Newton's methods leads to inexact Newton method.

$$\hat{R}(\hat{Q}) = 0 \qquad \left\|\hat{R}(\hat{Q}_k) + \hat{R}'(\hat{Q}_k)\,\Delta\hat{Q}_k\right\| \le \eta_k\left\|\hat{R}(\hat{Q}_k)\right\| \qquad \hat{R}'(\hat{Q}_k)\,\Delta\hat{Q}_k = -\hat{R}(\hat{Q}_k)$$

Results

Liquid Hydrocarbon fuels are more efficient in low hypersonic Mach numbers while Hydrogen is more efficient in high Mach numbers.

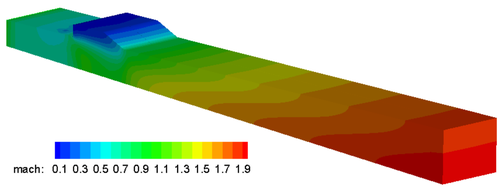

Figure 3. Combustor Mach number variation

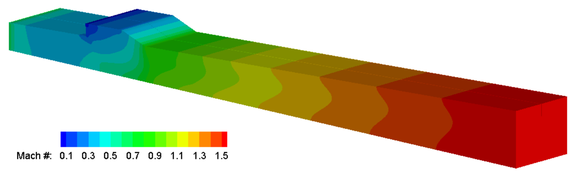

Figure 8. Combustor Mach number variation

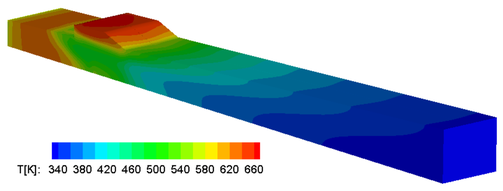

Figure 4. Combustor temperature distribution

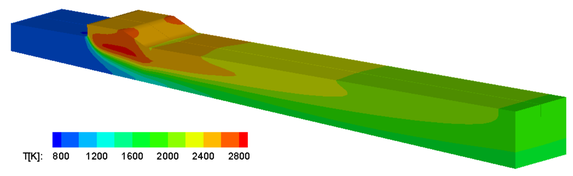

Figure 9. Combustor temperature distribution

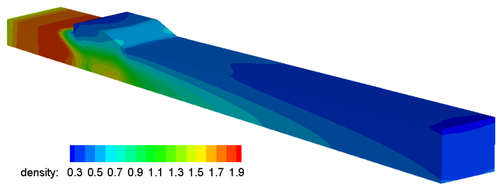

Figure 5. Combustor density distribution

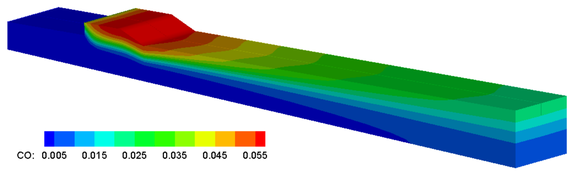

Figure 10. Hydroxide mass fraction

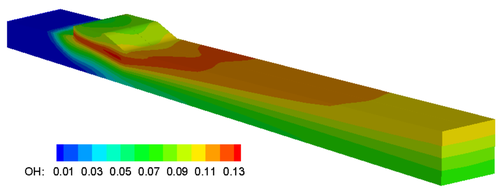

Figure 6. Hydroxide mass fraction

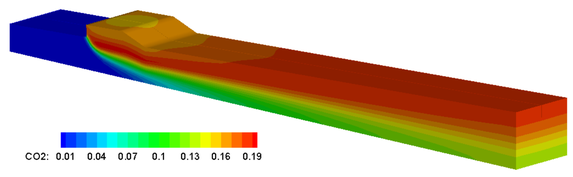

Figure 11. Hydroxide mass fraction

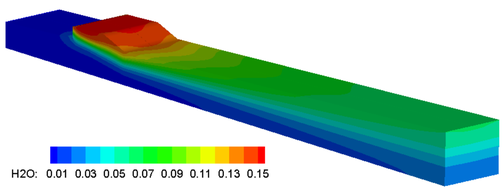

Figure 7. Vapor water mass fraction

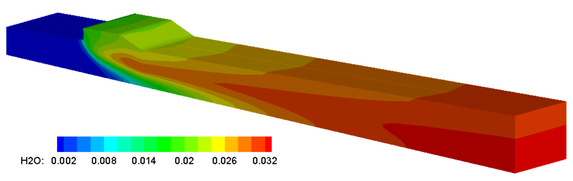

Figure 12. Vapor water mass fraction

Conclusions

Conclusion can be summarized as follows:

- A bow shock has been generated over the fuel injectors where velocity of the main flow decreases and density increased abruptly. Moreover, because of the recirculation region created in the cavity flow slows down further and so Mach number decreases. But, downstream of the cavity, velocity of the flow increased as a consequence of the divergent geometry of the combustion chamber.
- mixing occurs immediately after the injection of the fuel inside the cavity. The combustion process and decreasing flow velocity cause temperature to experience a peak, downstream of the fuel injectors in the cavity region.
- Mass fraction of the products increased after the fuel injection where combustion has occurred which is expected.

Acknowledgement

This research is supported by The Scientific and Technological Research Council of Turkey (TUBITAK).

Bibliography

1. Wang, Z., Wang, H., and Sun, M., "Review of cavity-stabilized combustion for scramjet applications," Proceedings of the Institution of Mechanical Engineers, Part G: Journal of Aerospace Engineering, vol. 228, Feb. 2014, pp. 2718–2735
2. Baurle, R. A., and Eklund, D. R., "Analysis of Dual-Mode Hydrocarbon Scramjet Introduction," vol. 18, 2002.
3. Lin, K., Tam, C., Carter, C., Jackson, K., and Lindsey, M., "Flame Characteristics and Fuel Entrainment Inside a Cavity Flame Holder in a Scramjet Combustor," 2007, pp. 1–19.